1st Latin-American Workshop on Structural Health Monitoring
LATAM-SHM 2023
December, 5-8 2023

A DATA DRIVEN FREQUENCY-DOMAIN VIRTUAL SENSING METHOD BASED ON CROSS-SPECTRAL DENSITY MATRICES

Marcos Nuñez*, Ricardo Prieto-Galarza†,‡ Christian Tutivén* and Luis David Avendaño-Valencia△

*Mechatronics Engineering
Faculty of Mechanical Engineering and Production Science, FIMCP
Escuela Superior Politécnica del Litoral, ESPOL
Campus Gustavo Galindo Km. 30.5 Vía Perimetral, P.O. Box 09-01-5863, Guayaquil, Ecuador
Phone number: +593 9 9103 5259
e-mail: {mnnunez, cjtutive}@espol.edu.ec
web page: https://www.espol.edu.ec

†Control, Data, and Artificial Intelligence, CoDAlab
Department of Mathematics, Escola d'Enginyeria de Barcelona Est, EEBE
Universitat Politècnica de Catalunya, UPC
Campus Diagonal-Besós (CDB) 08019, Barcelona, Spain
e-mail: ricardo.prieto@upc.edu,
Web page: https://www.upc.edu/es

‡Universidad Ecotec
Km. 13.5 Samborondón, Samborondón, EC092302 Ecuador

△Department of Mechanical and Electrical Engineering
University of Southern Denmark
Campusvej 55, 5230, Odense M, Denmark
Phone number: +4565504771
e-mail: ldav@sdu.dk
web page: https://www.sdu.dk/en

Key words: wind turbine drivetrains, condition monitoring, virtual sensing, cross spectral density

Abstract. Within the context of vibration-based condition monitoring, virtual sensing techniques facilitate vibration sensing at locations where sensors are not set at the time of inspection. In this work we postulate a data-driven frequency-domain virtual sensing procedure, based on *Cross Power Spectral Density* (CSD) matrices obtained from an initial dense sensor configuration. CSD matrices are used to build a conditional probability distribution for the Fourier transform of the withdrawn sensors, based on the response at the still available sensors, in a Gaussian process regression fashion. In this way, it is possible to estimate the Fourier transform of the vibration responses at the absent sensors, based on those from the available sensors. The proposed method is assessed in a wind turbine drivetrain diagnostics simulator, characterised by two speed reduction gearboxes (parallel shaft and planetary), and three shafts. The drivetrain is instrumented with accelerometers located on different bearings and on the

gearboxes. The full sensor set is used to build the reference CSD based on an initial dataset at a fixed speed and load. Later, the acceleration response at some of the sensors is estimated with the proposed virtual sensing method using measured responses from a limited set of accelerometers.

1 INTRODUCTION

In the domain of vibration-based structural health and condition monitoring (SHM/CM), the application of conventional physical sensors often presents substantial challenges, including the burdensome expenses associated with installation, procurement, and ongoing sensor maintenance. For instance, vibration-based CM of wind turbine drivetrains, where numerous components prone to failure but expensive to repair, the number of possible sensor locations is often very limited. Moreover, sensors must be located on the exterior of the machine, hindering the sensitivity towards feeble damage signatures.

An attractive alternative corresponds to virtual sensors, in which the response on locations where physical sensing is not possible, is extrapolated using information from other sensors [1, 2]. An evident advantage is that virtual sensing techniques operate exclusively within a digital environment, effectively mitigating the installation and maintenance costs associated with traditional physical sensors. In addition, virtual sensors can boost the sensing capabilities, facilitating response analysis in hard-to-reach locations, which can be used, among other things, for fatigue analysis and to increase damage diagnosis sensitivity [3, 4, 5].

Physics-based methods use information on the dynamics of the structure to extrapolate the vibration time series from available sensors to desired locations [2, 3, 6, 7]. Here, FE models, mode shapes and frequency response functions are typically used as a basis for virtual sensing. In data-driven methods, an initial dense sensor configuration is used to establish a model of the relation among sensors at different points in the structure. A sparse configuration is subsequently considered, after removing a subset of sensors. Then, the response at the withdrawn sensors can be extrapolated with the help of the model obtained in the first phase. Here, time-domain sensor correlation models [4, 5] or time-series models [1, 8] can be used.

In this work we postulate a data-driven frequency-domain virtual sensing procedure, based on *Cross power Spectral Density* (CSD) matrices obtained from an initial dense sensor configuration. The CSD matrices are interpreted as the frequency-domain covariance structure of the sensors, which is the basis to build a conditional probability distribution for the discrete Fourier transform of the withdrawn sensors, based on the response at the still available sensors, in a Gaussian process regression fashion. In this way, it is possible to estimate the Fourier transform of the vibration responses at the virtual positions, based on those from the available sensors. As a main contribution, in this work we introduce the technique based on Welch-based estimates of the CSD matrix, which allows estimation of the response of virtual sensors on N-sample signal blocks.

The proposed method is assessed in a wind turbine drivetrain diagnostics simulator, characterised by two speed reduction gearboxes (parallel shaft and planetary), and three shafts. The drivetrain is instrumented with accelerometers located on different bearings and on the gearboxes. The full sensor set is used to build the reference CSD matrix based on an initial dataset at a fixed speed and load. Later, the acceleration response at some of the sensors is

estimated with the proposed virtual sensing method, based on measured responses of a limited set of accelerometers.

The document is organized in the following manner. Section 2 details the proposed virtual sensor methodology. Section 3 describes the experimental setup, the assessed drivetrain operational and health conditions, and the data acquisition process. Section 4, describes the obtained results. Lastly, Section 5 provides the main conclusions and outlines directions for future research.

2 METHODOLOGICAL FRAMEWORK

The virtual sensing methodology postulated in this work uses the Cross Power Spectral Density (CSD) matrix as a frequency-domain reference of the relation among sensors in an SHM system. In this section, we first summarize the definition and estimation procedure of the CSD matrix, and subsequently, we introduce the CSD-based virtual sensing methodology.

2.1 Cross-power spectral density - Definition - Estimation

Main definitions: The *Power Spectral Density* (PSD) is a function indicating the distribution of the power (variance) of a stochastic process across frequency components. In simple terms, the PSD indicates the fraction of the power of a signal found in a frequency bin. Formally, for a discrete-time signal $x[t]$ $t \in \mathbb{Z}$, the PSD is defined as the Fourier transform of the signal's Auto-Correlation function $R_{xx}[\tau]$, $\tau \in \mathbb{Z}$, which is also equivalent to the expected value of the signal's Fourier transform squared magnitude as shown below [9, Sec. 5.2], [10, Sec. 8.3]:

$$P_{xx}(f) = \mathcal{F}\{R_{xx}[t]\} = E\{|X(f)|^2\} \tag{1}$$

where $X(f) := \mathcal{F}\{x[t]\}$, $f \in [-f_s/2, f_s/2]$ indicates the discrete-time Fourier transform of $x[t]$, f_s is the sampling rate in samples per time unit (*Hertz*), and $E\{\cdot\}$ is the expectation operator.

Analogously, the *Cross power Spectral Density* (CSD) between a pair of signals $x_i[t]$ and $x_j[t]$ is defined as the Fourier transform of the cross-correlation function between $x_i[t]$ and $x_j[t]$, namely $R_{x_i,x_j}[\tau]$. As in the case of the PSD, the CSD can also be calculated as the expected value of the product of the Fourier transforms $X_i(f) = \mathcal{F}\{x_i[t]\}$ and $X_j(f) = \mathcal{F}\{x_j[t]\}$. Both definitions are summarized below [9, Sec. 5.2], [10, Sec. 8.3]:

$$C_{x_i,x_j}(f) = \mathcal{F}\{R_{x_i,x_j}[t]\} = E\{X_i(f) \cdot X_j^*(f)\} \tag{2}$$

where the superscript $*$ indicates the complex conjugate.

Building upon the interpretation of the PSD, the CSD can be deemed as a way to quantify the co-dependency of the components of signals $x_i[t]$ and $x_j[t]$ around frequency f. Therefore, following from Eqns. (1) and (2), the PSD can be understood as the variance of the frequency component $X(f)$, while the CSD measures the cross-covariance of the frequency components $X_i(f)$ and $X_j(f)$.

Cross-Power Spectral Density Matrix: In the case of L concurrent signals organized in the vector $\boldsymbol{x}[t] = \begin{bmatrix} x_1[t] & x_2[t] & \cdots & x_L[t] \end{bmatrix}^T \in \mathbb{R}^L$, the CSD matrix is then defined as:

$$\boldsymbol{C_{xx}}(f) := E\{\boldsymbol{X}(f) \cdot \boldsymbol{X}^H(f)\} = \begin{bmatrix} C_{x_i,x_j}(f) \end{bmatrix} \in \mathbb{C}^{L \times L} \tag{3}$$

where $\boldsymbol{X}(f) = \mathcal{F}(\boldsymbol{x}[t])$ indicates the discrete-time Fourier transform of the vector signal $\boldsymbol{x}[t]$, and the superscript H indicates the *Hermitian* matrix, defined as the conjugate transpose matrix. The CSD matrix is composed by the PSD of each one of the individual signals $x_i[t]$ in the main diagonal, and the CSDs between signals $x_i[t]$ and $x_j[t]$ in the remainder of the matrix. Further details and properties of the PSD, CSD, and CSD matrix can be found, for instance, in [9, Ch. 5] or [10, Ch. 8].

Estimation of the CSD matrix: Estimation of the CSD matrix given the vector signal $\boldsymbol{x}[t] \in \mathbb{R}^L$ of finite length N_s (so that $t = 0, 1, 2, \ldots, N_s - 1$), can be accomplished via Welch's estimator. In short, Welch's estimate of the CSD between signals $x_i[t]$ and $x_j[t]$ is calculated as the average of the product the N-sample *Discrete Fourier Transforms* (DFTs) of each one of the signals on M blocks extracted concurrently from both signals, as explained below:

$$\hat{C}_{x_i,x_j}[n] = \frac{1}{NM}\sum_{m=1}^{M}(X_i^{(m)}[n]) \cdot (X_j^{(m)}[n])^* \qquad X_i^{(m)}[n] = \sum_{t=0}^{N-1} w[t] \cdot x_i^{(m)}[t] \cdot \mathrm{e}^{-j2\pi nt/N} \tag{4}$$

where $n = 0, 1, \ldots, N-1$ is the frequency index, $x_i^{(m)}[t]$ is a signal block of size N samples, and $w[t]$ $t = 0, 1, \ldots, N-1$ is a spectral window, which controls the effect of leakage in the DFT. Customarily, the signal blocks can be selected from overlapping segments on the available signal, so that the total number of averages used in the calculation of the PSD estimate is increased. Selection of the DFT size, overlap and type of spectral window are the adjustment parameters of the method, which are tuned to improve the quality of the result. Upon calculation of individual CSD estimates, the CSD matrix is built as follows:

$$\hat{\boldsymbol{C}}_{\boldsymbol{xx}}[n] = \left[\hat{C}_{x_i,x_j}[n]\right] \tag{5}$$

resulting in a complex-valued 3-dimensional tensor of dimensions $L \times L \times N$, providing the CSD matrix estimates at each one of the discrete frequency values $f_s n/N$, with $n = 0, 1, \ldots, N-1$.

2.2 CSD-based virtual sensing methodology

As explained in the previous section, the CSD can be interpreted as the frequency-domain covariance structure of a vector stochastic process. In this section, we exploit this property to estimate the DFT of the response at virtual sensors, based on a number of available sensor measurements, which follows from a Gaussian Process interpretation of the problem.

Frequency-domain vibration responses as Gaussian Process: A *Gaussian Process* (GP) represents a distribution over functions from a multivariate normal (Gaussian) distribution over all possible function values [11, Ch. 2],[12, Ch. 18]. This means that a function sampled at some point in space follows a normal distribution, whereas a set of sampling points in space follow a multivariate normal distribution.

In the present framework, we may define the frequency-domain vibration response across the structure as the complex-valued function $X(f, s) \in \mathbb{C}$, where f indicates frequency and s a spatial position. In turn, the measurements obtained at different sensor positions s_i, $i =$

$1, 2, \ldots, L$, are represented by the vector $\boldsymbol{X}(f) := \begin{bmatrix} X(f,s_1) & X(f,s_2) & \cdots & X(f,s_L) \end{bmatrix}^T \in \mathbb{C}^L$. Now, we define $X(f,s)$ as a GP with zero mean and covariance:

$$C(\{f,s\},\{f^*,s^*\}) = \delta(f-f^*)\cdot C_{x_s,x_{s^*}}(f) \tag{6}$$

where $\delta(f-f^*)$ designates the delta function, indicating no correlation between frequency components, and $C_{x_s,x_{s^*}}(f)$ indicates the CSD between the responses on positions s and s^* at frequency f. Based on this definition, the readings at the whole set of sensors in the vector $\boldsymbol{X}(f)$ follow the multivariate normal distribution, as shown below:

$$\begin{bmatrix} X(f,s_1) \\ X(f,s_2) \\ \vdots \\ X(f,s_L) \end{bmatrix} \sim \mathcal{N}\left(\begin{bmatrix} 0 \\ 0 \\ \vdots \\ 0 \end{bmatrix}, \begin{bmatrix} C_{11}(f) & C_{12}(f) & \cdots & C_{1L}(f) \\ C_{21}(f) & C_{22}(f) & \cdots & C_{2L}(f) \\ \vdots & \vdots & \ddots & \vdots \\ C_{L1}(f) & C_{L2}(f) & \cdots & C_{LL}(f) \end{bmatrix} \right) \quad \Rightarrow \quad \boldsymbol{X}(f) \sim \mathcal{N}\left(\boldsymbol{0}_n, \boldsymbol{C_{xx}}(f)\right) \tag{7}$$

where $C_{ij}(f) \equiv C_{x_i,x_j}(f)$.

Virtual sensing: We may now define the virtual sensing problem, as the problem of calculating the vibration responses at some *virtual* positions contained in the vector $\boldsymbol{X}_v(f) \in \mathbb{C}^{L_v}$ based on some *available* sensor readings in the vector $\boldsymbol{X}_a(f) \in \mathbb{C}^{L_a}$. Following from Eq. (7), we define the vector $\boldsymbol{X}(f) = \begin{bmatrix} \boldsymbol{X}_a^T(f) & \boldsymbol{X}_v^T(f) \end{bmatrix}^T$, which leads to the following partition of the multivariate normal distribution:

$$\begin{bmatrix} \boldsymbol{X}_a(f) \\ \boldsymbol{X}_v(f) \end{bmatrix} \sim \mathcal{N} \begin{bmatrix} \boldsymbol{0}_{n_a} \\ \boldsymbol{0}_{n_v} \end{bmatrix} \begin{bmatrix} \boldsymbol{C_{aa}}(f) & \boldsymbol{C_{av}}(f) \\ \boldsymbol{C_{va}}(f) & \boldsymbol{C_{vv}}(f) \end{bmatrix} \tag{8}$$

where $\boldsymbol{C_{aa}}(f) \in \mathbb{C}^{L_a \times L_a}$ is the CSD matrix of the available sensors, $\boldsymbol{C_{av}}(f) = \boldsymbol{C_{av}}^H(f) \in \mathbb{C}^{L_a \times L_v}$ is the CSD matrix calculated between the available and virtual sensors, and $\boldsymbol{C_{vv}}(f) \in \mathbb{C}^{L_v \times L_v}$ is the CSD matrix of the virtual sensors.

Using the property of conditional probability for the multivariate normal distribution, we can then calculate an estimate of the response on the virtual sensors given the available sensors, $\hat{\boldsymbol{X}}_{v|a}(f)$ and its covariance $\boldsymbol{C}_{v|a}(f)$, as the conditional expectations:

$$\hat{\boldsymbol{X}}_{v|a}(f) = E\left\{\boldsymbol{X}_v(f) \,|\, \boldsymbol{X}_a(f)\right\} = \boldsymbol{C_{va}}(f)\cdot \boldsymbol{C_{aa}}^{-1}(f)\cdot \boldsymbol{X}_a(f) \tag{9a}$$

$$\boldsymbol{C}_{v|a}(f) = E\{\boldsymbol{X}_v(f)\cdot \boldsymbol{X}_v^H(f) \,|\, \boldsymbol{X}_a(f)\} = \boldsymbol{C_{vv}}(f) - \boldsymbol{C_{va}}(f)\cdot \boldsymbol{C_{aa}}^{-1}(f)\cdot \boldsymbol{C_{va}}^H(f) \tag{9b}$$

Accordingly, the virtual sensor estimate $\hat{\boldsymbol{X}}_{v|a}(f)$ corresponds to the mean value of $\boldsymbol{X}_v(f)$ given $\boldsymbol{X}_a(f)$, while the CSD matrix $\boldsymbol{C}_{v|a}(f)$ quantifies the uncertainty remaining in the virtual sensor estimate as a function of frequency. The latter can be interpreted as the reliability of the virtual sensor estimates across the frequency axis. In turn, the quantity $\boldsymbol{C_{va}}(f)\cdot \boldsymbol{C_{aa}}^{-1}(f)\cdot \boldsymbol{C_{av}}(f)$ can be deemed as the best estimate of the CSD matrix $\boldsymbol{C_{vv}}(f)$ based on the information of the available sensors.

Application of the algorithm based on the DFT: Practical application of the algorithm is based on experimentally obtained CSD matrix estimates $\hat{\boldsymbol{C}}_{aa}[n]$, $\hat{\boldsymbol{C}}_{va}[n]$ and $\hat{\boldsymbol{C}}_{vv}[n]$ on the discrete frequencies $n = 0, 1, \ldots, N-1$, based on Welch estimates, as explained in Sec. 2.1. This implies that on a *training* phase, the CSD matrices are obtained based on the complete array of sensors, including the sensor positions that will become virtual sensors in normal operation. Subsequently, on *normal operation*, the N-sample DFTs estimates of the response at virtual sensors $\hat{\boldsymbol{X}}_v[n]$ are calculated based on the respective N-sample DFTs of the measured responses at available sensors $\hat{\boldsymbol{X}}_a[n]$. Time-domain responses on the virtual sensors are ultimately found as the inverse DFT of the obtained frequency-domain estimates. The obtained methodology is summarized in Fig. 1.

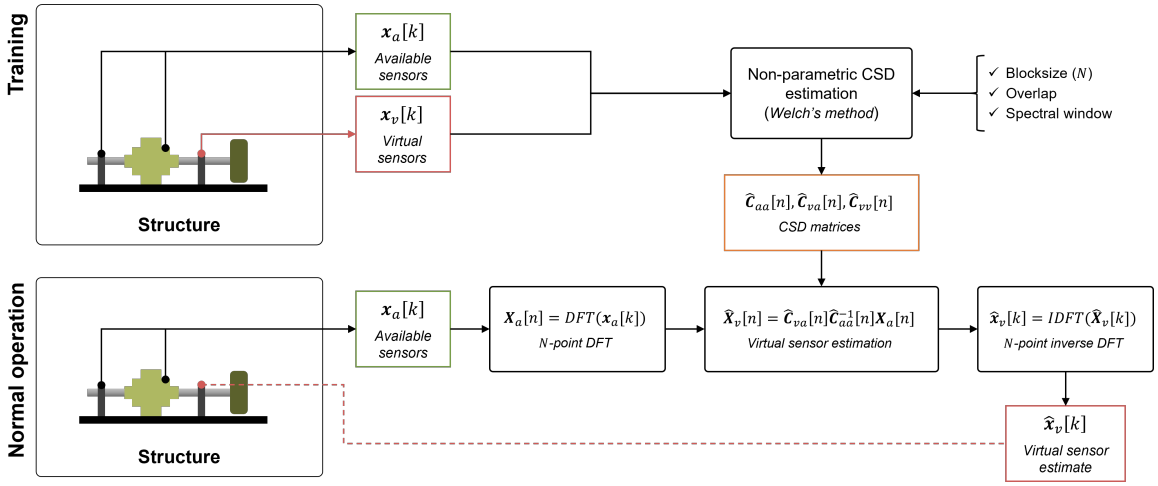

Figure 1: Summary of the CSD-based virtual sensing methodology

3 APPLICATION STUDY

Experimental setup The analysis presented here is based on vibration data extracted from a *Drivetrain Diagnostics Simulator* (DDS), manufactured by SpectraQuest, shown in Figure 2, and further described in [13]. The DDS was designed to simulate industrial wind turbine drivetrains for experimental and educational purposes. The studied DDS system consists of an electric motor located on the left side driven with a speed/torque regulator where it applies torque to the transmission via the high speed shaft (HSS), which is transferred to the parallel shaft gearbox for a first speed reduction stage, leading to the medium speed shaft (MSS). The MSS is connected to a planetary gearbox which further reduces the rotational speed towards the low speed shaft (LSS). The LSS is connected to a controllable load, in the form of a pair of programmable electromagnetic brakes. Each one of the three shafts (HSS, MSS, LSS) includes couplers (yellow boxes in Figure 2) designed to break apart the sides of the shafts, and thus facilitate the exchangeability and modularity of the drivetrain components. Bearings 1 (located at MSS) and 2 (located at LSS), are the relevant parts in this case study because these are the ones that are exchanged to simulate the different types of failures.

The DDS is instrumented with seven piezoelectric accelerometers (S1 to S7) placed at different parts of the drivetrain and an optical encoder mounted on the MSS, which provides a

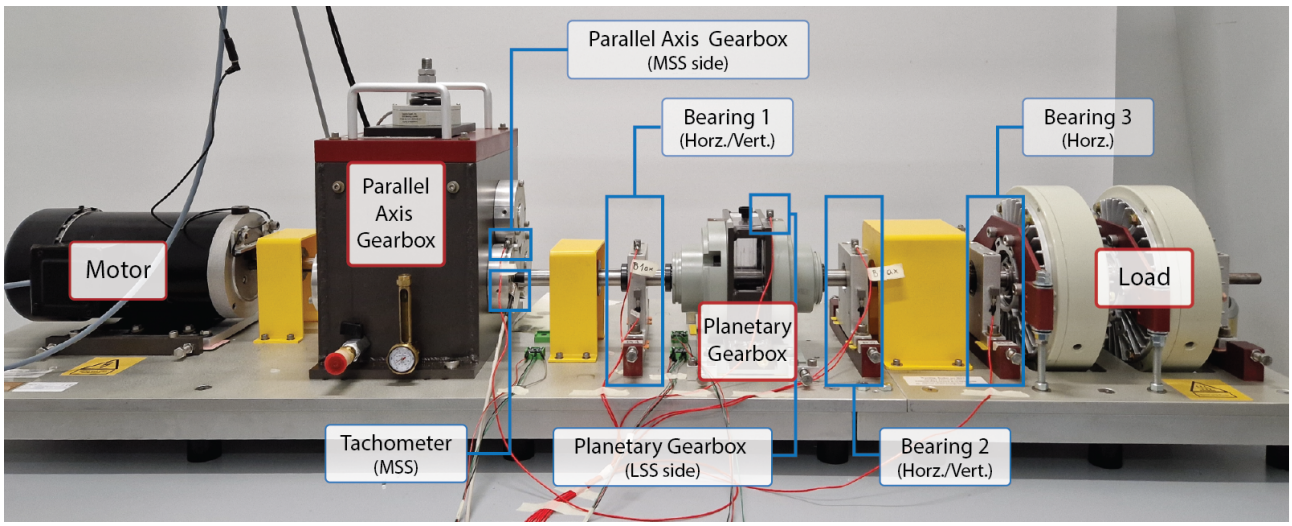

Figure 2: Wind turbine drivetrain diagnostic simulator with main components and sensor locations [13].

reference tachometer signal. The accelerometers used in this study are Dytran 3097A22 uniaxial IEPE accelerometers with a sensitivity of ~ 100 mV/g and a 50 g measuring range. The accelerometers are distributed along the drivetrain, in the positions indicated in Table 1. The sensors are located on critical parts of the drivetrain, where damages are most likely to occur, namely the bearings and gearboxes.

Location	Description	Name
Bearing 1	Two accelerometers on the horizontal and vertical axis, mounted on the side and top respectively.	S1-S2
Bearing 2	Two accelerometers on the horizontal and vertical axis, mounted on the side and top respectively.	S3-S4
Bearing 3	One accelerometer on the horizontal axis mounted on the side.	S5
Parallel axis gearbox	One accelerometer mounted on the medium speed output shaft.	S6
Planetary gearbox	One accelerometer mounted towards on the low speed output shaft over the ring gear.	S7

Table 1: Location of the accelerometers in the DDS system.

Condition	Description	Name
Healthy	All bearings are in good condition.	H
Damage 1	Bearing 1: outer race failure, bearing 2: healthy.	D1

Table 2: List of health conditions introduced in the DDS system.

Data acquisition In the present study, the analysis focuses on two health conditions of the DDS, namely a healthy condition and damage in one of the bearings, as indicated in Table

2. Further, two rotational speeds (10 and 16 Hz) and two load conditions (0% and 40%) are considered as well. For each of these configurations described above, 30 experiments of 60 seconds each are carried out at a sampling frequency of 5120 Hz.

CSD estimation CSD matrices are estimated using Welch's method, as explained in Sec. 2.1, using the following settings: Hann window with DFT size $N = 4192$, number of overlapping samples 2048 and resulting number of averages of the CSD estimator 74. As a result, CSD tensors of dimensions $7 \times 7 \times N$ are obtained for each one of the drivetrain operating conditions are calculated.

Configuration of virtual sensing Once CSD matrices are estimated for the complete array of sensors, sensors 1 to 6 are kept as available sensors, while sensor 7 is set as virtual sensor. Then, based on the obtained CSD matrices, estimates of the DFT of the response at the virtual sensor of size N are calculated using Eq. (9a).

4 RESULTS

4.1 Results in frequency domain

The results of the DFT of the virtual sensor for the DDS system under the healthy condition operating at 10 Hz and 0% load (orange lines) compared with the DFT of the actual sensor readings (blue lines) are shown in Fig. 3. Corresponding results for the DDS under bearing 1 outer race failure operating at 10 Hz and 0% load are shown in Fig. 4.

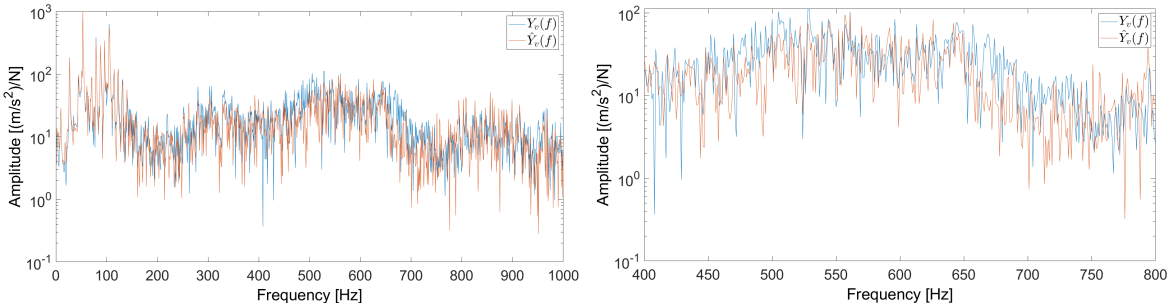

Figure 3: DFT virtual sensor estimate in position 7 in the full frequency range (left), and detailed view from 400 to 800 Hz (right). Condition corresponding to healthy state at 10Hz and 0% load.

In both cases, a good match between the DFTs of the actual sensor reading and the virtual sensor estimate are found through most of the frequency axis. Detailed analysis on the frequency range from 400 to 800 Hz for the healthy case indicate larger discrepancies within this frequency range. Such discrepancies are interpreted as dynamics that are particular to the specific sensor (sensor 7: planetary gearbox) and cannot be correlated to the other sensors. Similar analysis on the damaged case, indicates slightly better compliance of the virtual sensor estimation with the actual signal.

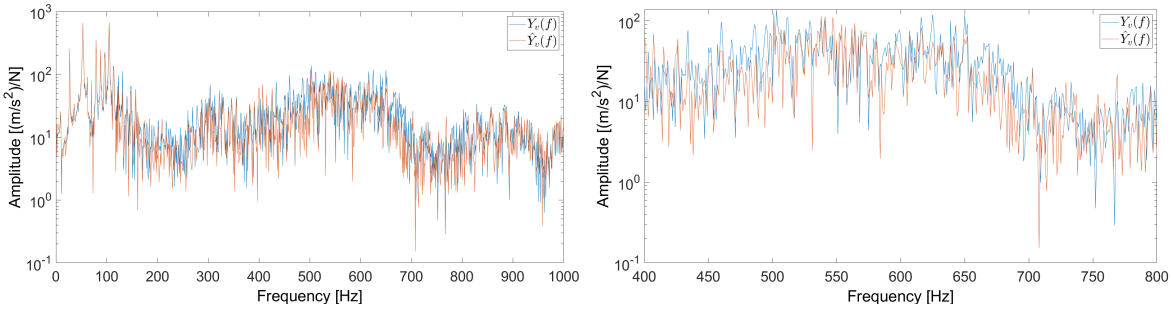

Figure 4: DFT virtual sensor estimate in position 7 in the full frequency range (left), and detailed view from 400 to 800 Hz (right). Condition corresponding to bearing 1 outer race failure at 10Hz and 0% load.

4.2 Results in time domain

Fig. 5 provides the sensor signals transformed back in time domain for the healthy (left) and damaged (right) conditions of the drivetrain operating at 10 Hz and 0% load. The results show that the waveforms of the actual and virtual sensor signals are very similar, while the instantaneous squared error shows that the error seems to have a periodic pattern, which again is interpreted as the unique dynamic characteristics found on sensor 7.

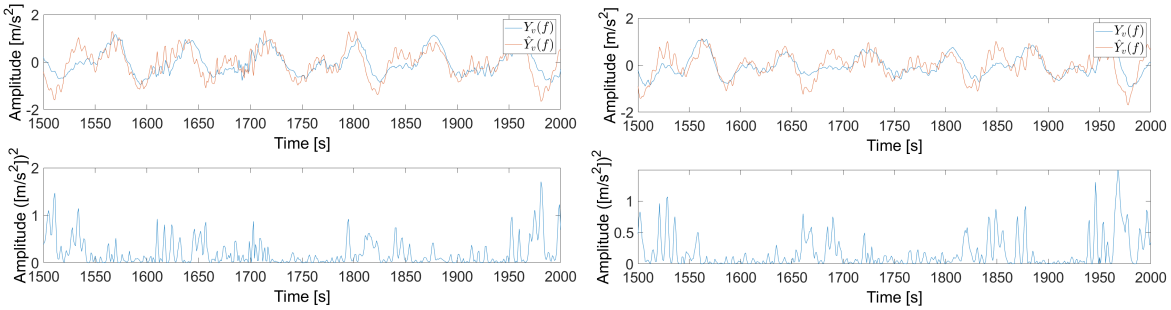

Figure 5: Time domain analysis of the sensor responses at the healthy condition (left) and damaged condition (right) operating at 10Hz and 0% load. Top row displays the virtual and actual sensor readings, bottom row provides the instantaneous squared error between these signals.

4.3 Error analysis

The virtual sensor estimation procedure is repeated for all the 30 individual experiments at each health and operational condition and the Mean Squared Error (MSE) is calculated at each of those cases. The distributions of the obtained MSE at all the considered conditions, displayed as boxplots, are shown in Fig. 6. Overall, it is observed that the error distribution stays within a similar range in the healthy and damaged states across all the drivetrain conditions. Nonetheless, the median value of the MSE tends to change according to the operational condition of the drivetrain, with largest values observed in the 10 Hz 40% load.

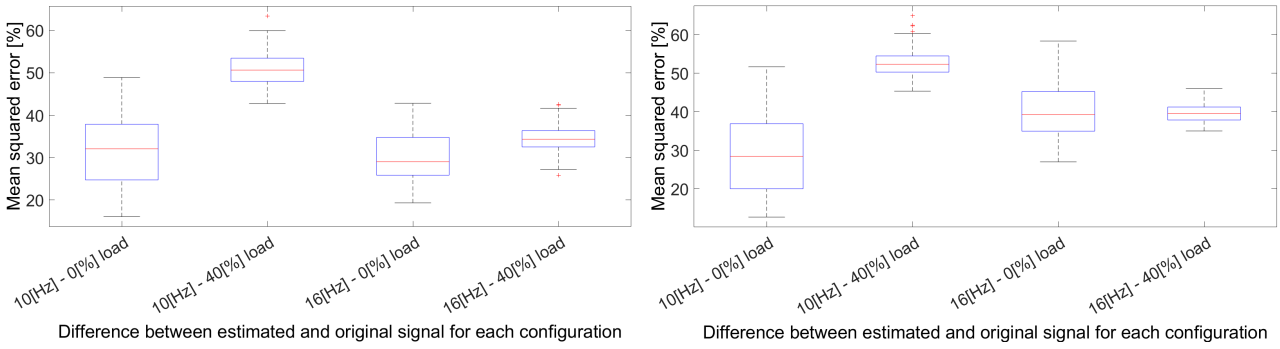

(a) Healthy H1 state (b) Damage D1 state

Figure 6: MSE boxplots for virtual sensor estimates across the 30 individual experiments at different DDS configurations.

5 CONCLUSIONS

By using cross-spectral density matrices, it was possible to develop a virtual sensor capable of successfully estimating the original signals of the available physical sensors. Thus, by means of their frequency domain plots, particular characteristics of each configuration established in each experiment were identified, which are very useful to be able to relate the different sensors present with unique behaviours that can be related either to the dynamics of their structure or to the operating conditions of their environment. The results obtained have revealed a consistent error range, oscillating between 20% and 40% approximately for most of the models evaluated. This range of error is in line with the expectations set at the beginning of the project since a model is used as a starting point to estimate the different sensors. This project lays the foundations for future research and improvements in the different techniques used to optimise and calibrate the models in order to significantly reduce the error intervals. On the other hand, these models can incorporate advanced techniques with machine learning approaches in order to further improve the accuracy of the obtained estimates that can be implemented for damage detection and prevention, which is so necessary nowadays in these types of fields where costs for maintenance or machinery failures are so high but need immediate attention because more and more clean, sustainable energy sources are needed and that is why this approach is based on WT transmission systems.

REFERENCES

[1] N. Dimitrov, T. Göçmen, Virtual sensors for wind turbines with machine learning-based time series models, Wind Energy 25 (9) (2022) 1626–1645.

[2] J. Kullaa, Virtual sensing of structural vibrations using dynamic substructuring, Mechanical Systems and Signal Processing 79 (2016) 203–224.

[3] V. Flores Terrazas, O. Sadehi, C. Papadimitriou, L. S. Katafygiotis, A streamline approach to multiaxial fatigue monitoring using virtual sensing, Structural Control and Health Monitoring 29 (2022) e2863.

[4] J.-J. Wang, Y.-H. Zheng, L.-B. Zhang, L.-X. Duan, R. Zhao, Virtual sensing for gearbox condition monitoring based on kernel factor analysis, Petroleoum Science 14 (2017) 539–548.

[5] J. Kullaa, Robust damage detection in the time domain using Bayesian virtual sensing with noise reduction and environmental effect elimination capabilities, Journal of Sound and Vibration 473 (2020) 115232.

[6] B. M. Castro, U. A. Monteiro, R. H. Gutiérrez, Comparison of vibration response prediction on the main deck of a catamaran using experimental, numerical and correlated mode shapes, Marine Structures 89 (2023) 103371.

[7] S. Oh, H. Lee, J.-K. Lee, H. Yoon, J.-G. Kim, Real-time response estimation of structural vibration with inverse force identification, Structural Control and Health Monitoring (2023) 2691476.

[8] Z. Yue, L. Liu, T. Long, Y. Ma, Virtual sensing method for monitoring vibration of continuously variable configuration structures using long short-term memory networks, Chinese Journal of Aeronautics 33 (2020) 244–254.

[9] J. S. Bendat, A. G. Piersol, Random Data: Analysis and Measurement Procedures, 4th Edition, John Wiley and Sons, 2010.

[10] A. Brandt, Noise and Vibration Analysis: Signal Analysis and Experimental Procedures, 1st Edition, John Wiley and Sons, 2010.

[11] C. Rasmussen, Gaussian Processes for Machine Learning, MIT Press, 2006.

[12] A. Zhang, Z. C. Lipton, M. Li, A. J. Smola, Dive into Deep Learning, Cambridge University Press, 2023, `https://D2L.ai`.

[13] L. D. Avendaño-Valencia, A. Georgantopoulou, A fast identification algorithm for Linear Parameter Varying Vector AR models of short-term drivetrain vibration, in: D. Saravanos, A. Benjeddou, N. Chrysochoidis, T. Theodosiou (Eds.), Eccomas Proceedia SMART, 2023, pp. 1–12. `doi:10.7712/150123.9865.451289`.